AIChE

Reaction Mechanism and Kinetics for the Liquid-phase Catalytic Oxidation of *meta*-Xylene to *meta*-Phthalic Acid

Qinbo Wang
College of Chemistry and Chemical Engineering, Hunan University, Changsha, 418002 Hunan, People's Republic of China, and Dept. of Chemical Engineering, Zhejiang University, Hangzhou, 310027 Zhejiang, People's Republic of China

Yongzhao Zhang
Dept. of Chemical Engineering, Hangzhou Vocational and Technical College, Hangzhou, 310027 Zhejiang, People's Republic of China

Youwei Cheng and Xi Li
Dept. of Chemical Engineering, Zhejiang University, Hangzhou, 310027 Zhejiang, People's Republic of China

DOI 10.1002/aic.11574
Published online July 22, 2008 in Wiley InterScience (www.interscience.wiley.com).

A detailed radical chain elementary reaction mechanism for the liquid-phase catalytic oxidation of meta-xylene to meta-phthalic acid catalyzed by cobalt acetate and manganese acetate and promoted by hydrogen bromide was proposed. Using several reasonable assumptions a simple fractional-like kinetic model was derived from the assumed reaction mechanism. Several batch oxidation experiments were carried out to study the oxidation kinetics. The experiments included three values of the initial concentration of meta-xylene and four values of reaction temperature. The developed model parameters were determined in a nonlinear optimization, minimizing the difference between the simulated and experimental time evolutions of the product compositions obtained in a batch oxidation reactor, where the gas and liquid phases were well mixed. The experimental results cannot be interpreted by the empirical n-th order kinetics, but can be interpreted by the kinetic model proposed in this work. It means the kinetic model proposed in this work reveals the reaction mechanism. © 2008 American Institute of Chemical Engineers *AIChE J,* 54: 2674–2688, 2008

Keywords: catalytic oxidation, radical chain elementary reaction mechanism, kinetics, meta-*xylene,* meta-*phthalic acid*

Introduction

As one of the most important aromatic compounds, *meta*-phthalic (MPA) is widely used in organic synthesis, particularly in the polyester and paint industry. Commercially, the majority of MPA is produced by the air oxidation of *meta*-xylene (MX) in acetic acid (HAc) in the temperature range from 448.2 to 473.2 K, catalyzed by cobalt acetate ($Co(Ac)_2$) and manganese acetate ($Mn(Ac)_2$) and promoted by hydrogen bromide (HBr).[1–4] To gain better insight into the reaction mechanism and identify the effects of different parameters on the progress of the reaction, it is essential to study the kinetics. Further, the rational design, optimization,

Correspondence concerning this article may be addressed to any author. Q. Wang's e-mail addresses are wang_qinbo@vip.163.com and wang_qinbo@hun.cn. Y. Cheng's e-mail address is ywcheng@zju.edu.cn and X. Li's e-mail address is lixi@zju.edu.cn.

control, and analysis of the oxidation of MX to MPA process also require knowledge of the reaction mechanism and kinetics.

The liquid-phase catalytic oxidation of MX to MPA in acetic acid media is a typical aromatic hydrocarbon oxidation process, which belongs to the kind of classical free-radical chain reaction. Researchers such as Kamiya,[5] Hendriks et al.,[6] Jones,[7–9] Hronec et al.,[10,11] Partenheimer et al.,[12–18] Suresh et al.,[19,20] Harustiak et al.,[21,22] George and Steven,[23] Sheldon and Kochi,[24] Wang et al.,[25,26] Emanuel and Gal,[27] Marta et al.,[28] Wang et al.,[29] and Cheng[30] had studied the mechanism of aromatic hydrocarbon liquid-phase catalytic oxidation for many years. In the oxidation of methyl aromatic hydrocarbon to aromatic carboxylic acid, a mixture of cobalt(II), manganese(II) and bromide salts, which can be called 'Mid-century' catalysts, are used as catalyst species. It is well established that these metal catalysts, with reduction potentials of -42 and -35 kcal/mol for Co(III) and Mn(III), respectively, can produce radical species of methylaromatics compounds.[24] The bromine radical, $Br^{\bullet}$, with a redox potential of -25 kcal mol, is less powerful than either Co(III) or Mn(III), but is known to generate benzylic radicals($RCH_2^{\bullet}$).[13] The rate of benzylic radical generation is much faster with Br than either Co(III) or Mn(III). The initiation mechanism is predominantly hydrogen abstraction from methyl groups by bromine atoms. The Mn and Co ions oxidize the bromine ions formed to bromine atoms thus ensuring the availability of bromine atoms for initiation.[31] Although different in some specific chain elementary reactions, the following general free-radical chain elementary reactions involving the initiation, propagation, and termination steps are commonly accepted[14,31]:

$$M^{3+} + Br^- \rightarrow M^{2+} + Br^{\bullet}$$
$$Br^{\bullet} + RCH_3 \rightarrow RCH_2^{\bullet} + H^+ + Br^-$$
$$RCH_2^{\bullet} + O_2 \rightarrow RCH_2O_2^{\bullet}$$
$$RCH_2O_2^{\bullet} + M^{2+} \rightarrow RCHO + M^{3+} + OH^-$$
$$RCHO + M^{3+} \rightarrow RCO^{\bullet} + M^{2+} + H^+$$
$$RCHO + Br^{\bullet} \rightarrow RCO^{\bullet} + Br^- + H^+$$
$$RCO^{\bullet} + O_2 \rightarrow RCO_3^{\bullet}$$
$$RCO_3^{\bullet} + RH \rightarrow RCO_3H + R^{\bullet}$$
$$RCO_3H + RCHO \rightarrow 2RCOOH$$
$$RCO_3H + M^{2+} \rightarrow RCO_2^{\bullet} + M^{3+} + OH^-$$
$$RCO_2^{\bullet} + RH \rightarrow RCOOH + R^{\bullet}$$
$$I_i^{\bullet} + I_i^{\bullet} \rightarrow I_i^{\bullet} \rightarrow I_iI_j$$

where *M* denotes metal catalyst such as Co or Mn, *R* denotes aromatic reactants and *I* denotes radicals produced. Here, the initial step is thought to be the generation of $Br^{\bullet}$ radical and the hydrogen abstraction illustrated in the first two reactions. The propagation step consists of oxidation of the substrates by molecular oxygen, metal ion and $Br^{\bullet}$ radical, and reduction of radicals and hydroperoxides by metal ion. The termination step consists of reactions between two radicals.

The complexity of the chain elementary reactions clearly prevents the evaluation of the individual values of the kinetic constant by direct fitting of the model results against the experimental data. Furthermore, the formulation of detailed kinetic models of the complex process which describes all the involved radical chain elementary reactions and all the intermediate products is not desirable in practice. This is mainly because the estimation of the kinetics parameters of the radical chain reactions by fitting of the experimental data are very difficult to be performed when the concentrations of the participating components (that is, the radical species in the liquid phase) are very difficult to be measured. To low the computing efforts, the most common approach is to lump the detailed mechanism into a set of global reactions, which involves only molecular species. The concentrations of these molecular species can be, in principle, easily monitored as a function of time.[32–35] Without involving formal procedure of general validity but simply including the minimum number of reactions to describe the behavior of all the species of interest, but by accounting for the most important intermediates and final products of the process, i.e. MX, *meta*-tolualdehyde (*m*-TALD), *meta*-toluic acid (*m*-TA), *meta*-carboxybenzaldehyde (*m*-CBA), and MPA, the lumped kinetic scheme shown in Figure 1 for the liquid-phase oxidation of MX to TA was proposed,[1–4] where the reactions of MX to *m*-TALD and *m*-TA to *m*-CBA involve the addition of $1O_2$ and the reactions of *m*-TALD to *m*-TA and m-CBA to MPA involve the addition of $1/2O_2$. The lumped kinetics scheme may have important practical applications in the production of MPA.

Zhang studied the liquid-phase catalytic oxidation kinetic of *m*-TA to MPA catalyzed by cobalt acetate and manganese acetate and promoted by tetrabromoethane at 453.2–473.2 K.[1] He empirically assumed that all the reactions were *n*-th order with respect to liquid reactants. The correlated results showed that the oxidation of *m*-TA to *m*-CBA was 0.3-th order with respect to *m*-TA and the oxidation of *m*-CBA to MPA was 0.35-th order with respect to *m*-CBA. The averaged relative deviation between the experimental and model correlated data was 12.8%. The studies on temperature effects showed that the activation energies for the oxidation of *m*-TA and *m*-CBA are almost the same.

Wan studied the liquid-phase catalytic oxidation kinetic of MX to MPA catalyzed by Co/Mn/Br at 448.2–473.2 K.[4] He also empirically assumed that all the reactions were *n*-th order with respect to liquid reactants. The correlated results showed that the oxidation of MX to *m*-TALD was 0.87-th order with respect to MX, and the oxidation of *m*-TALD to *m*-PT was 0.5-th order with respect to *m*-TALD, and the oxidation of *m*-TA to *m*-CBA was 0.75-th order with respect to *m*-TA, and the oxidation of *m*-CBA to MPA was 0.54-th order with respect to *m*-CBA. The averaged relative deviation between the experimental and model correlated data was not given. The studies on temperature effects showed that the activation energies of the four oxidation steps shown in Figure 1 ranged from 28.4 to 156.7 kJ/mol. Among them, the activation energy of *m*-PT to *m*-CBA was the highest and that of *m*-CBA to MPA was the second highest. Catalytic oxidation of *m*-TA to *m*-CBA was the control step of the reaction system. However, when the *n*-th reaction kinetics was used in an industrial oxidation process, there was a significant difference between the simulated results and the industrial operating results. It was

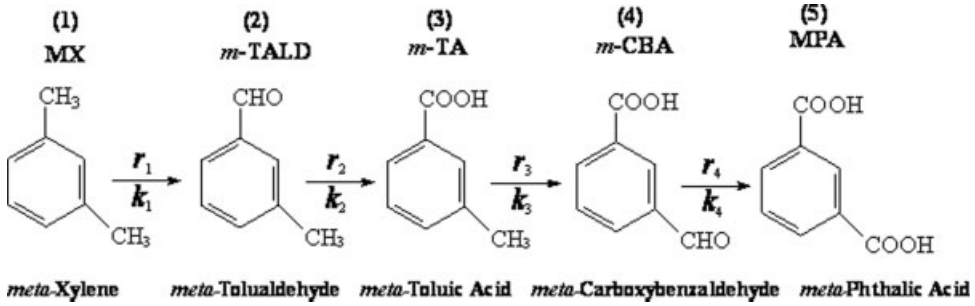

Figure 1. Lumped kinetic scheme for the oxidation of *meta*-xylene to *meta*-phthalic acid.

mainly because the kinetics previously obtained was empirical and did not reveal the reaction mechanism sufficiently. A kinetic model derived from the reaction mechanism is necessary.

Wang et al.[25,26] and Cheng[30] developed a kinetic model as shown in Eq. 1 from the radical chain elementary reaction mechanisms for the liquid-phase catalytic oxidation of *para*-xylene to terephthalic acid

$$r_j = \frac{k_j c_j}{(d_{1j}c_1 + d_{2j}c_2 + d_{3j}c_3 + d_{4j}c_4 + \varepsilon_j)^{\beta j}} \quad j = 1-4 \quad (1)$$

where k_j is the reaction rate constant and is affected by temperature, catalyst concentration and ratio, etc. The d_{ij}, β_j and ε_j are model parameters. Zhang et al. assumed that the kinetic models for the liquid-phase catalytic oxidation of MX to MPA were similar with that of *para*-xylene to terephthalic acid, and Eq. 1 could be used as the kinetic model for the oxidation to MPA,[2,3] because they thought that the molecular structure for *para*-xylene and MX are similar, and the oxidation condition, catalyst and solvent system, reaction path are also similar for the liquid-phase catalytic oxidation of *para*-xylene to terephthalic acid and MX to MPA. Based on the assumed kinetic model, they studied the liquid-phase catalytic oxidation kinetic of MX to MPA catalyzed by Co/Mn/Br at 453.2–473.2 K and the model parameters in Eq. 1 were obtained by the fitting of experimental data. The fitting results showed that the activation energies of the four oxidation steps shown in Figure 1 ranged from 40 to 76 kJ/mol. Among them, the activation energy of *m*-CBA to MPA was the highest and that of *m*-TA to *m*-CBA was the second highest. Catalytic oxidation of *m*-CBA to *m*-TA was the control step of the reaction system. However, one needs to be careful about the assumption made by Zhang et al.[2,3] The oxidation of *para*-xylene and MX are significantly different in two aspects. The solubility of the oxidation products of terephthalic acid and MPA are quite different. MPA is roughly 10 times more soluble than terephthalic acid. This means that the rate of metal-catalyzed decarboxylation of MPA is 10 times more important than terephthalic acid.[36] The metal-catalyzed decarboxylation is a deactivation mechanism because it is in direct competition with Co(III) for Br and Mn(II). Also radicals form in the para-position on the benzene ring are resonance stabilized, whereas those in the meta-position are not. Therefore decomposition of these radicals to by-products such as carbon dioxide might be higher in MX oxidation than in *para*-xylene oxidation.[36]

The kinetic model and model parameters reported in public literatures are quite different, and even somewhere contradictory. This might mainly because the available kinetic models proposed are all not derived from the reaction mechanism of MX to MPA, but empirical. The available literature is not complete when one looks for mechanism and kinetics for the liquid-phase catalytic oxidation of MX to MPA. There exists a scope and a necessity to propose a detailed radical chain elementary reaction mechanism, and the kinetic model derived from the reaction mechanism is preferred. This is just the aim of this work, and the work consists of two parts. In the first part, a radical chain reaction mechanism will be proposed. Based on the proposed mechanism, a fractional-like kinetics model will be derived. In the second part, experiments results on the oxidation process will be discussed, and the model parameters in the proposed kinetics will be determined by data fitting.

Experimental Work

Apparatus and procedure

The experimental apparatus used in this work appears in Figure 2. The 0.5 L oxidation reactor was constructed from titanium to resist corrosion and was designed for temperatures up to 493 K and pressures up to 30 atm. A paddle-type agitator with a turbine impeller is used for agitation. The system was equipped with three condensers in order to ensure complete condensation and recycle of the evaporated compounds. The pressure was controlled by a back-pressure valve to be 16 atm. A Pt100 thermal resistance thermometer was inserted into the reactor for the measurement of temperature, and the thermometer had a measurement range from 423.15 to 493.15 K and had an uncertainty of ± 0.1K. The details about the experimental apparatus have been described by Cheng et al.[37]

In each experiment, the liquid reactant MX, solvent acetic acid, and catalysts Co/Mn/Br were batch deposited in the reactor at room temperature. The solution in the reactor was heated at about 10 K/min to the experimental temperature. The temperature was maintained within ± 0.5 K of the desired temperature by a PID controlling system shown in Figure 2. When the temperature was higher than the desired point, the computer program would start the peristaltic pump, and cooling oil would flow through the spiral cooling coil in

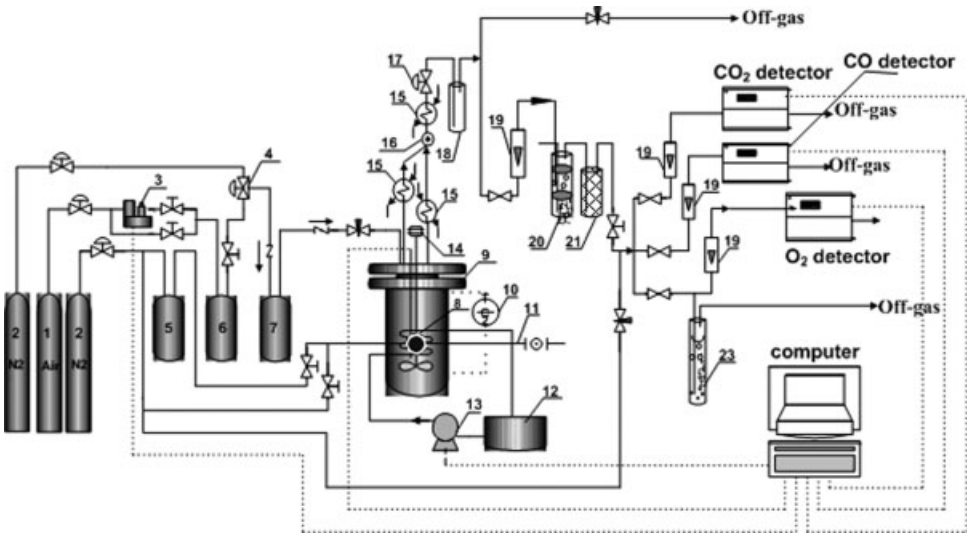

Figure 2. Experimental apparatus for the oxidation of *meta*-xylene to *meta*-phthalic acid.

1. air tank, 2. nitrogen tank, 3. mass flowmeter, 4. air inlet valve, 5. solvent DMSO pot, 6. air buffer drum, 7. air buffer pot, 8. sampler, 9. reactor, 10. heating control circuit, 11. sample cell, 12. cooling oil tank, 13. peristalic pump, 14. agitator, 15. condenser, 16. peephole, 17. back-pressure valve, 18. gas-liquid separator, 19. rotameter, 20. scrubber, and 21. dryer

the reactor to cool the content in the reactor. When the temperature was lower than the desired point, the computer program would start the heating controlling circuit, and the reactor wall would be electrically heated. When the solution temperature was heated to the experimental point, the gaseous reactant air was continuously fed into the reactor, and the oxidation began. The experimental conditions are listed in Table 1, while fixing the reaction pressure at 1.6 MPa, and the oxygen volume fraction in the vent at no less than 4%, and the initial mass percent of water at 0%. In these experiments, Run 1–3 were carried out to study the effect of initial reactant concentration on the oxidation process, and Runs 2 and 4–6 were carried out to study the effect of temperature on the oxidation process, and Runs 2 and 7–8 were carried out to study the effect of stirring rate on the oxidation process.

During the oxidation process, the reaction slurry was sampled every 0.5–2.5 min. MX oxidation occurs at high temperature and high pressure. The loss of light components due to volatilization, and the plugging of sampling pipes and valves due to the crystallization of heavy components make the sampling operation difficult and the samples distorted. In our experiments, a gear drag-bar sampler as illustrated in Figure 3 was used to sample the reaction slurry at high temperatures and pressures. The sampling technique can avoid the loss of light components due to volatilization and the plugging of sampling pipes and valves due to the crystallization. On the bottom of the sampling rod there were a "⊥" hole entryway and a horizontal hole entryway. The diameter of each hole was 1.5 mm. One could pull the sampling rod out of the reactor to a fixed position so that the "⊥" hole could be connected with the sample cell. At this moment the solution in the reactor would flow into the sample cell at the system pressure until the sample cell was filled with liquid-phase sample. It should be emphasized that at this moment the outlet valve, the carrier gas valve and the solvent valve should be closed. Then one could push the sampling rod into the reactor, so that the sample was enclosed in the sampling cell. To avoid the loss of solvents by evaporation, the sample was cooled to room temperature quickly by the water cooling jacket surrounding the sample cell, in which most of the solute would crystallize. Then the outlet valve and the carrier gas valve were open, and the samples in the sample cell were swept out by the purged nitrogen into a sampling collector. To collect the crystallized solute into the sampling collector, the solvent valve was open, and the sample cell was flushed by the solvent dimethyl sulfoxide at least three

Table 1. Operating Conditions for the Experimental Runs

Run	*T* (K)	MX/HAc (mass ratio)	Co (ppm)	Co/Mn/Br (atom ratio)	Stirring Rate (rpm)
1	463.2	0.20	200	1/3/3	900
2	463.2	0.10	200	1/3/3	900
3	463.2	0.05	200	1/3/3	900
4	453.2	0.10	200	1/3/3	900
5	458.2	0.10	200	1/3/3	900
6	468.2	0.10	200	1/3/3	900
7	463.2	0.10	200	1/3/3	600
8	463.2	0.10	200	1/3/3	750

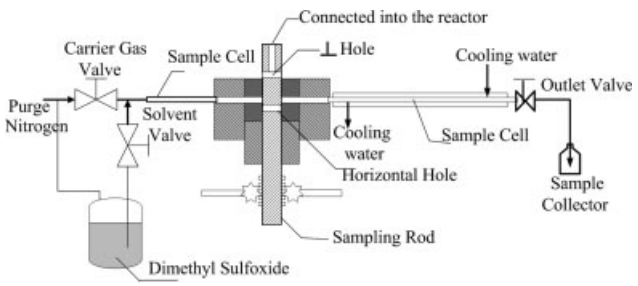

Figure 3. Sketch of the sampler.

times. In each measurement about 1–2 mL of the saturated solution was sampled. Some dimethyl sulfoxide was added to the sample to dissolve all the crystallized solutes. Some isopropyl benzene (IPB), acting as the internal standard substance, was also added to the sample, and the solution was diluted to 25 mL with methanol. The sample was then analyzed using the method introduced in the following section.

Analytical techniques

The internal standard method was used in the analysis.The liquid reactant MX, liquid intermediates *m*-TALD, *m*-PT, *m*-CBA, and product MPA in the solution were analyzed by high-performance liquid chromatograph (HPLC). The mass ratio of liquid components to the internal standard substances in the solution was determined. The column of Diamonsil C18 (250 mm $\times$ 4.6 mm, Φ5 μm) was used in the analysis. Gradient elution was used for complete separation of the analytes at room temperature. The mobile phase consisted of three eluents (i.e. water + acetonitrile + methanol), and the following three-component gradient evolution program was adopted: At 0 min, 5 mass % acetonitrile and 95% water; From 0 to 5 min, the mixture composition changed linearly with time to become 85 mass % water, 5 mass % methanol, and 10 mass % acetonitrile; From 5 to 8 min, the mixture composition changed linearly with time to become 55 mass % water, 10 mass % methanol and 35 mass % acetonitrile; From 8 to 12 min, the mixture composition changed linearly with time to become 15 mass % water, 10 mass % methanol and 75 mass % acetonitrile; From 12 to 14 min, the mixture composition changed linearly with time to become pure acetonitrile; From 14 min on, 100 mass % acetonitrile. Each analysis took about 20 min.

The mass ratio of solvent HAc to the internal standard substances in the solution was determined by a Shimadzu GC-9A GC with a hydrogen flame ionization detector. The SE-54(30 m) capillary chromatographic column was used. In the experiments, IPB was used as the internal standard substance to correlate the data obtained from GC and HPLC analysis.

To verify the uncertainty of the concentration measurement, two MPA + *m*-CBA + *m*-PT +*m*-TALD + MX + IPB + HAc solutions of known concentration were analyzed. Compared with the known concentration, the uncertainty of concentration was less than 3.0% of the known concentration. To check the reproducibility, the two solutions were measured at least five times, and the reproducibility evaluated with a mean relative deviation of less than 3.0%.

Reaction Mechanism and Kinetic Model

Reaction mechanism

Elucidation of the reaction mechanism helps in selecting more efficient catalysts, optimizing the reaction intermediates, selecting reaction conditions, and designing of a commercial reactor. This process also generates ideas for further research and development. The oxidation of hydrocarbons is usually explained in terms of the classical free-radical chain mechanism involving the initiation, propagation, and termination steps.[31]

The catalytic oxidation of aromatic hydrocarbon by cobalt(II) and manganese(II) salts can be characterized by an induction period in which Co(II) and Mn(II) are oxidized to Co(III) and Mn(III). Monomeric Co(III) and Mn(III) are powerful oxidizing agents when they are surrounded by O-donor ligands such as water, OH- ions, or RCOO— ions, and can produce radical species of methylaromatic compounds.[24] The reactions can be illustrated by

$$\mathrm{Co(III)} + \mathrm{R{-}Ph{-}CH_3} \longrightarrow \mathrm{R{-}Ph{-}CH_2^{\bullet}} + \mathrm{H^+} + \mathrm{Co(II)} \quad (2)$$

$$\mathrm{Mn(III)} + \mathrm{R{-}Ph{-}CH_3} \longrightarrow \mathrm{R{-}Ph{-}CH_2^{\bullet}} + \mathrm{H^+} + \mathrm{Mn(II)} \quad (3)$$

The bromine radical, $Br^{\bullet}$, with a redox potential of -25 kcal mol, is less powerful than either Co(III) or Mn(III), but is known to generate benzylic radicals($R{-}Ph{-}CH_2^{\bullet}$).[13] The reaction can be illustrated by

$$\mathrm{Br^{\bullet}} + \mathrm{R-Ph-CH_3} \longrightarrow \mathrm{R-Ph-CH_2^{\bullet}} + H^+ + \mathrm{Br^-} \quad (4)$$

The rate of $R{-}Ph{-}CH_2^{\bullet}$ generation is much faster with $Br^{\bullet}$ than either Co(III) or Mn(III). It means in the oxidation process, the rates of reaction (4) is much faster than that of reactions (2) and (3), and the radical reactions (2) and (3) can be neglected. Partenheimer has emphasized that these two metals greatly enhance the selectivity of the oxidation i.e, reduce by-product formation.[13,14,31] The addition of cobalt by itself greatly reduces the rate of generation of the unselective carbon dioxide, carbon monoxide, and cresols as well as decarboxylation products such as toluene. The addition of Br to Co, further increase the selectivity of the reaction (as well as the activity) by reducing the steady-state concentration of Co(III) through the following reaction[13,14,38]:

$$\mathrm{Co(III)} + \mathrm{Br^-} \xrightarrow{k_1} \mathrm{Co(II)} + \mathrm{Br^{\bullet}} \quad (5)$$

The effect of Mn addition to Co/Br increases the activity and selectivity to the catalyst through the following reactions[13,14,38]:

$$\mathrm{Co(III)} + \mathrm{Mn(II)} \xrightarrow{k_2} \mathrm{Co(II)} + \mathrm{Mn(III)} \quad (6)$$

$$\mathrm{Mn(III)} + \mathrm{Br^-} \xrightarrow{k_3} \mathrm{Mn(II)} + \mathrm{Br^{\bullet}} \quad (7)$$

We can conclude that the initiation mechanism is predominantly hydrogen abstraction from methyl groups by $Br^{\bullet}$ (see Eq. 4). The Mn and Co ions oxidize the bromine ions formed to bromine radical thus ensuring the availability of bromine radical for initiation (see Eqs. 5–7).[31] $Br^{\bullet}$ radical is the reaction initiator, and the radical chain propagation and termination reactions from MX to MPA can be illustrated by the following reactions. To simplify the treatment, similar to that for the oxidation of *para*-xylene to terephthalic acid,[29] some assumptions are necessary: (a) there is no inclusion of $RCH_2O^{\bullet}$ and $^{\bullet}OH$ radicals in the propagation and termination steps; (b) chain termination takes places by reactions of $Br^{\bullet}$ radical and other active radicals, and other radicals are not allowed to undergo termination reactions.

Oxidation of MX to m-*TALD*. $Br^{\bullet}$ radical initiates the oxidation of MX by hydrogen abstraction from MX through the

following radical reaction:

$$Br^{\bullet} + m\text{—}CH_3\text{—}Ph\text{—}CH_3 \xrightarrow{k_4} m\text{—}CH_3\text{—}Ph\text{—}CH_2^{\bullet} + H^+ + Br^- \quad (8)$$

where Ph denotes the benzene ring, *m* denotes the *meta*-substituted group. The generated $m\text{—}CH_3\text{—}Ph\text{—}CH_2^{\bullet}$ radical has high reactivity and can be combined with molecular oxygen quickly to generate $m\text{—}CH_3\text{—}Ph\text{—}CH_2O_2^{\bullet}$ radical by the reaction

$$m\text{—}CH_3\text{—}Ph\text{—}CH_2^{\bullet} + O_2 \xrightarrow{k_5} m\text{—}CH_3\text{—}Ph\text{—}CH_2O_2^{\bullet} \quad (9)$$

and then the following six parallel radical reactions may occur

$$m\text{—}CH_3\text{—}Ph\text{—}CH_2O_2^{\bullet} + Co(II) + H^+ \xrightarrow{k_6} m\text{—}CH_3\text{—}Ph\text{—}CHO + Co(III) + H_2O \quad (10)$$

$$m\text{—}CH_3\text{—}Ph\text{—}CH_2O_2^{\bullet} + Mn(II) + H^+ \xrightarrow{k_7} m\text{—}CH_3\text{—}Ph\text{—}CHO + Mn(III) + H_2O \quad (11)$$

$$m\text{—}CH_3\text{—}Ph\text{—}CH_2O_2^{\bullet} + Co(II) + H^+ \longrightarrow m\text{—}CH_3\text{—}Ph\text{—}CH_2OOH + Co(III) \quad (12)$$

$$m\text{—}CH_3\text{—}Ph\text{—}CH_2O_2^{\bullet} + Mn(II) + H^+ \longrightarrow m\text{—}CH_3\text{—}Ph\text{—}CH_2OOH + Mn(III) \quad (13)$$

$$m\text{—}CH_3\text{—}Ph\text{—}CH_2O_2^{\bullet} + RCH_3 \longrightarrow m\text{—}CH_3\text{—}Ph\text{—}CH_2OOH + RCH^{\bullet} \quad (14)$$

$$m\text{—}CH_3\text{—}Ph\text{—}CH_2O_2^{\bullet} + HAC \longrightarrow m\text{—}CH_3\text{—}Ph\text{—}CH_2OOH + (AC)^{\bullet} \quad (15)$$

The hydroperoxide $m\text{—}CH_3\text{—}Ph\text{—}CH_2OOH$ generated by reaction (12)–(15) is unstable and may be decomposed by Co(II) or Mn(II) through the following two reactions

$$m\text{—}CH_3\text{—}Ph\text{—}CH_2OOH + Co(II) + H^+ \longrightarrow m\text{—}CH_3\text{—}Ph\text{—}CH_2O^{\bullet} + Co(III) + H_2O \quad (16)$$

$$m\text{—}CH_3\text{—}Ph\text{—}CH_2OOH + Mn(II) + H^+ \longrightarrow m\text{—}CH_3\text{—}Ph\text{—}CH_2O^{\bullet} + Mn(III) + H_2O \quad (17)$$

In the oxidation of *para*-xylene to terephthalic acid, the following six elementary reactions also occur

$$p\text{—}CH_3\text{—}Ph\text{—}CH_2O_2^{\bullet} + Co(II) + H^+ \longrightarrow p\text{—}CH_3\text{—}Ph\text{—}CHO + Co(III) + H_2O \quad (10')$$

$$p\text{—}CH_3\text{—}Ph\text{—}CH_2O_2^{\bullet} + Mn(II) + H^+ \longrightarrow p\text{—}CH_3\text{—}Ph\text{—}CHO + Mn(III) + H_2O \quad (11')$$

$$p\text{—}CH_3\text{—}Ph\text{—}CH_2O_2^{\bullet} + Co(II) + H^+ \longrightarrow p\text{—}CH_3\text{—}Ph\text{—}CH_2OOH + Co(III) \quad (12')$$

$$p\text{—}CH_3\text{—}Ph\text{—}CH_2O_2^{\bullet} + Mn(II) + H^+ \longrightarrow p\text{—}CH_3\text{—}Ph\text{—}CH_2OOH + Mn(III) \quad (13')$$

$$p\text{—}CH_3\text{—}Ph\text{—}CH_2O_2^{\bullet} + RCH_3 \longrightarrow p\text{—}CH_3\text{—}Ph\text{—}CH_2OOH + RCH^{\bullet} \quad (14')$$

$$p\text{—}CH_3\text{—}Ph\text{—}CH_2O_2^{\bullet} + HAC \longrightarrow p\text{—}CH_3\text{—}Ph\text{—}CH_2OOH + (AC)^{\bullet} \quad (15')$$

Partenheimer reported that the rates of reaction (10′) and (11′) were much faster than that of reaction (12′)–(15′).[12–18] The oxidation of *para*-xylene to terephthalic acid is similar with the oxidation of MX to MPA, and the two oxidation process all belong to the classical radical chain elementary reactions. Here, for the oxidation of MX to MPA, we can also assume that the rates of reaction (10) and (11) were much faster than that of reactions (12)–(15), which resulted in most of the methyl group were oxidized into aldehyde group directly, and the radical reactions (12)–(17) could be neglected when only the main reactions were considered. In this sense, the oxidation of MX to *m*-TALD can be expressed by the radical chain elementary reactions (5)–(11) and the major radicals are $Br^{\bullet}$, $m\text{—}CH_3\text{—}Ph\text{—}CH_2^{\bullet}$ and $m\text{—}CH_3\text{—}Ph\text{—}CH_2O_2^{\bullet}$.

The major chain termination reactions are that between two radicals.[6,11] Because $Br^{\bullet}$ radical acts the most important role in chain initiation and propagation, here only the following reactions between $Br^{\bullet}$ radical and other radicals are considered as the chain termination reactions

$$Br^{\bullet} + m\text{—}CH_3\text{—}Ph\text{—}CH_2^{\bullet} \xrightarrow{k_8} m\text{—}CH_3\text{—}Ph\text{—}CH_2Br \quad (18)$$

$$Br^{\bullet} + m\text{—}CH_3\text{—}Ph\text{—}CH_2O_2^{\bullet} \xrightarrow{k_9} m\text{—}CH_3\text{—}Ph\text{—}CH_2O_2Br \quad (19)$$

Oxidation of m-*TALD to* m-*TA* The aromatic aldehyde group also can be oxidized to the corresponding peroxide radical $RCO_3^{\bullet}$ in the same manner as that of methyl group, and then reacts with divalent metal ion to generate aromatic peracid RCOOOH.[25,26,30] The specific reactions may be as follows

$$Br^{\bullet} + m\text{—}CH_3\text{—}Ph\text{—}CHO \xrightarrow{k_{10}} m\text{—}CH_3\text{—}Ph\text{—}CO^{\bullet} + H^+ + Br^- \quad (20)$$

$$m\text{—}CH_3\text{—}Ph\text{—}CO^{\bullet} + O_2 \xrightarrow{k_{11}} m\text{—}CH_3\text{—}Ph\text{—}CO_3^{\bullet} \quad (21)$$

$$m\text{—}CH_3\text{—}Ph\text{—}CO_3^{\bullet} + Co(II) + H^+ \xrightarrow{k_{12}} m\text{—}CH_3\text{—}Ph\text{—}COOOH + Co(III) \quad (22)$$

$$m\text{—}CH_3\text{—}Ph\text{—}CO_3^{\bullet} + Mn(II) + H^+ \xrightarrow{k_{13}} m\text{—}CH_3\text{—}Ph\text{—}COOOH + Mn(III) \quad (23)$$

The reducibility of aldehyde group is strong and the following self-catalyzed Baeyer-Villiger reaction between aldehyde group and aromatic peracid may occur to generate aromatic acid[24,27]

$$m\text{—}CH_3\text{—}Ph\text{—}COOOH + m\text{—}CH_3\text{—}Ph\text{—}CHO \xrightarrow{k_{14}} 2m\text{—}CH_3\text{—}Ph\text{—}COOH \quad (24)$$

Besides the way to generate the aromatic acid via the Baeyer-Villiger reaction (see reaction Eq. 24), the peroxyacid reacts with Co(II) or Mn(II) and also gives the aromatic acid by the following reactions[7,16,36]

$$m\text{—}CH_3\text{—}Ph\text{—}COOOH + 2Co(II) + 2H^+ \xrightarrow{k_{15}} m\text{—}CH_3\text{—}Ph\text{—}COOH + 2Co(III) + H_2O \quad (25)$$

$$m\text{—}CH_3\text{—}Ph\text{—}COOOH + 2Mn(II) + 2H^+ \xrightarrow{k_{16}} m\text{—}CH_3\text{—}Ph\text{—}COOH + 2Mn(III) + H_2O \quad (26)$$

The oxidation of *m*-TALD to *m*-TA can be expressed by the radical chain reactions (20)–(26) and the major radicals and peracid in the oxidation of *m*-TALD to *m*-TA are $Br^{\bullet}$, $m\text{—}CH_3\text{—}Ph\text{—}CO^{\bullet}$, $m\text{—}CH_3\text{—}Ph\text{—}CO_3^{\bullet}$, and $m\text{—}CH_3\text{—}Ph\text{—}COOOH$. Here also only the following reactions between $Br^{\bullet}$ radical and other radicals are considered as the chain termination reactions.

$$Br^{\bullet} + m\text{—}CH_3\text{—}Ph\text{—}CO^{\bullet} \xrightarrow{k_{17}} m\text{—}CH_3\text{—}Ph\text{—}COBr \quad (27)$$

$$Br^{\bullet} + m\text{—}CH_3\text{—}Ph\text{—}CO_3^{\bullet} \xrightarrow{k_{18}} m\text{—}CH_3\text{—}Ph\text{—}CO_3Br \quad (28)$$

Oxidation of m-*TA to* m-*CBA*. Similar to the oxidation of MX to *m*-TALD, the oxidation of *m*-TA to *m*-CBA also belongs to the oxidation of methyl group to aldehyde group, and the following radical chain reactions might occur according to that of (8)–(11) and (18)–(19)

$$Br^{\bullet} + m\text{—}HOOC\text{—}Ph\text{—}CH_3 \xrightarrow{k_{19}} m\text{—}HOOC\text{—}Ph\text{—}CH_2^{\bullet} + H^+ + Br^- \quad (29)$$

$$m\text{—}HOOC\text{—}Ph\text{—}CH_2^{\bullet} + O_2 \xrightarrow{k_{20}} m\text{—}HOOC\text{—}Ph\text{—}CH_2O_2^{\bullet} \quad (30)$$

$$m\text{—}HOOC\text{—}Ph\text{—}CH_2O_2^{\bullet} + Co(II) + H^+ \xrightarrow{k_{21}} m\text{—}HOOC\text{—}Ph\text{—}CHO + Co(III) + H_2O \quad (31)$$

$$m\text{—}HOOC\text{—}Ph\text{—}CH_2O_2^{\bullet} + Mn(II) + H^+ \xrightarrow{k_{22}} m\text{—}HOOC\text{—}Ph\text{—}CHO + Mn(III) + H_2O \quad (32)$$

$$Br^{\bullet} + m\text{—}HOOC\text{—}Ph\text{—}CH_2^{\bullet} \xrightarrow{k_{23}} m\text{—}HOOC\text{—}Ph\text{—}CH_2Br \quad (33)$$

$$Br^{\bullet} + m\text{—}HOOC\text{—}Ph\text{—}CH_2O_2^{\bullet} \xrightarrow{k_{24}} m\text{—}HOOC\text{—}Ph\text{—}CH_2O_2Br \quad (34)$$

Oxidation of m-*CBA to MPA*. Similar to the oxidation of *m*-TALD to *m*-TA, the oxidation of *m*-CBA to MPA also belongs to the oxidation of aldehyde group to carboxy group, and the following radical chain reactions might occur according to that of (20)–(28)

$$Br^{\bullet} + m\text{—}HOOC\text{—}Ph\text{—}CHO \xrightarrow{k_{25}} m\text{—}HOOC\text{—}Ph\text{—}CO^{\bullet} + H^+ + Br^- \quad (35)$$

$$m\text{—}HOOC\text{—}Ph\text{—}CO^{\bullet} + O_2 \xrightarrow{k_{26}} m\text{—}HOOC\text{—}Ph\text{—}CO_3^{\bullet} \quad (36)$$

$$m\text{—}HOOC\text{—}Ph\text{—}CO_3^{\bullet} + Co(II) + H^+ \xrightarrow{k_{27}} m\text{—}HOOC\text{—}Ph\text{—}COOOH + Co(III) \quad (37)$$

$$m\text{—}HOOC\text{—}Ph\text{—}CO_3^{\bullet} + Mn(II) + H^+ \xrightarrow{k_{28}} m\text{—}HOOC\text{—}Ph\text{—}COOOH + Mn(III) \quad (38)$$

$$m\text{—}HOOC\text{—}Ph\text{—}COOOH + m\text{—}CH_3\text{—}Ph\text{—}CHO \xrightarrow{k_{29}} 2m\text{—}HOOC\text{—}Ph\text{—}COOH \quad (39)$$

$$m\text{—}HOOC\text{—}Ph\text{—}COOOH + 2Co(II) + 2H^+ \xrightarrow{k_{30}} m\text{—}HOOC\text{—}Ph\text{—}COOH + 2Co(III) + H_2O \quad (40)$$

$$m\text{—}HOOC\text{—}Ph\text{—}COOOH + 2Mn(II) + 2H^+ \xrightarrow{k_{31}} m\text{—}HOOC\text{—}Ph\text{—}COOH + 2Mn(III) + H_2O \quad (41)$$

$$Br^{\bullet} + m\text{—}HOOC\text{—}Ph\text{—}CO^{\bullet} \xrightarrow{k_{32}} m\text{—}HOOC\text{—}Ph\text{—}COBr \quad (42)$$

$$Br^{\bullet} + m\text{—}HOOC\text{—}Ph\text{—}CO_3^{\bullet} \xrightarrow{k_{33}} m\text{—}HOOC\text{—}Ph\text{—}CO_3Br \quad (43)$$

There must be many other chain reactions that are not considered in the above mechanism, but the radical chain reactions (2)–(43) might be expected to approximately represent the reaction mechanism for the oxidation of MX to MPA.

Kinetic model

The oxidation of MX to MPA is a typical consecutive reaction, and coupling effects exist among reactants, radicals and catalyst. Rounded consideration of these interactions is necessary for the mechanistic kinetic model establishment. In this work, by accounting for the most important intermediates and final products of the process as shown in Figure 1, the reaction rates of MX, *m*-TALD, *m*-TA, *m*-CBA, and MPA are considered. According to the reaction scheme

(Figure 1) and mechanism reaction (8), the consumption rate for MX may be determined as

$$\frac{d[\mathrm{MX}]}{dt} = -r_1 = -k_4[\mathrm{MX}][\mathrm{Br}^\bullet] \tag{44}$$

According to the reaction scheme (Figure 1) and the mechanism reactions (20) and (24), the generating rate for *m*-TALD may be determined as

$$\frac{d[m\text{-TALD}]}{dt} = r_1 - r_2 = r_1 - [m\text{-TALD}](k_{10}[\mathrm{Br}^\bullet] + k_{14}[m\text{—}\mathrm{CH_3}\text{—Ph—COOOH}]) \tag{45}$$

According to the reaction scheme (Figure 1) and the mechanism reactions (29), the generating rate for *m*-TA may be determined as

$$\frac{d[m\text{-TA}]}{dt} = r_2 - r_3 = r_2 - k_{19}[m\text{-TA}][\mathrm{Br}^\bullet] \tag{46}$$

According to the reaction scheme (Figure 1) and the mechanism reactions (35) and (39), the generating rate for *m*-CBA may be determined as

$$\frac{d[m\text{-CBA}]}{dt} = r_3 - r_4 = r_3 - [m\text{-CBA}](k_{25}[\mathrm{Br}^\bullet] + k_{29}[m\text{—HOOC—Ph—COOOH}]) \tag{47}$$

The major radicals produced in the radical chain reactions (2)–(43) are $Br^\bullet$, $m\text{—}CH_3\text{—Ph—}CH_2^\bullet$, $m\text{—}CH_3\text{—Ph—}CH_2O_2^\bullet$, $m\text{—}CH_3\text{—Ph—}CO^\bullet$, $m\text{—}CH_3\text{—Ph—}CO_3^\bullet$, $m\text{—HOOC—Ph—}CH_2^\bullet$, $m\text{—HOOC—Ph—}CH_2O_2^\bullet$, $m\text{—HOOC—Ph—}CO^\bullet$, and $m\text{—HOOC—Ph—}CO_3^\bullet$, and the aromatic peroxyacid produced in reactions (2)–(36) are $m\text{—}CH_3\text{—Ph—COOOH}$ and $m\text{—HOOC—Ph—COOOH}$. From reactions (5), (7), (8), (18)–(20), (27)–(29), (33)–(35), and (42)–(43), the generating rate of $Br^\bullet$ radical may be determined as

$$\frac{d[\mathrm{Br}^\bullet]}{dt} = (k_1[\mathrm{Co}^{3+}] + k_3[\mathrm{Mn}^{3+}])[\mathrm{Br}^-] - (k_4[\mathrm{MX}] + k_{10}[m\text{—TALD}] + k_{19}[m\text{—TA}] + k_{25}[m\text{—CBA}] + [\mathrm{I}^\bullet])[\mathrm{Br}^\bullet] \tag{48}$$

where

$$[I^\bullet] = k_8[m\text{—}CH_3\text{—Ph—}CH_2^\bullet] + k_9[m\text{—}CH_3\text{—Ph—}CH_2O_2^\bullet] + k_{17}[m\text{—}CH_3\text{—Ph—}CO^\bullet] + k_{18}[m\text{—}CH_3\text{—Ph—}CO_3^\bullet] + k_{23}[m\text{—HOOC—Ph—}CH_2^\bullet] + k_{24}[m\text{—HOOC—Ph—}CH_2O_2^\bullet] + k_{32}[m\text{—HOOC—Ph—}CO^\bullet] + k_{33}[m\text{—HOOC—Ph—}CO_3^\bullet] \tag{49}$$

represents the linear assembled total concentration of all the reactive radicals that are produced in the oxidation process.

From reactions (8), (9), and (18), the generating rate of $m\text{—}CH_3\text{—Ph—}RCH_2^\bullet$ radical may be determined as

$$\frac{d[m\text{—}CH_3\text{—Ph—}CH_2^\bullet]}{dt} = k_4[\mathrm{MX}][\mathrm{Br}^\bullet] - (k_5[\mathrm{O_2}] + k_8[\mathrm{Br}^\bullet])[m\text{—}CH_3\text{—Ph—}CH_2^\bullet] \tag{50}$$

From reactions (9)–(11) and (19), the generating rate of $m\text{—}CH_3\text{—Ph—}RCH_2O_2^\bullet$ radical may be determined as

$$\frac{d[m\text{—}CH_3\text{—Ph—}CH_2O_2^\bullet]}{dt} = k_5[\mathrm{O_2}][m\text{—}CH_3\text{—Ph—}CH_2^\bullet] - (k_6[\mathrm{Co}^{2+}][\mathrm{H}^+]) + k_7[\mathrm{Mn}^{2+}][\mathrm{H}^+] + k_9[\mathrm{Br}^\bullet])[m\text{—}CH_3\text{—Ph—}CH_2O_2^\bullet] \tag{51}$$

From reactions (20), (21), and (27), the generating rate of $m\text{—}CH_3\text{—Ph—}CO^\bullet$ radical may be determined as

$$\frac{d[m\text{—}CH_3\text{—Ph—}CO^\bullet]}{dt} = k_{10}[m\text{-TALD}][\mathrm{Br}^\bullet]\text{—}(k_{11}[\mathrm{O_2}] + k_{17}[\mathrm{Br}^\bullet])[m\text{—}CH_3\text{—Ph—}CO^\bullet] \tag{52}$$

From reactions (21)–(23) and (28), the generating rate of $m\text{—}CH_3\text{—Ph—}CO_3^\bullet$ radical may be determined as

$$\frac{d[m\text{—}CH_3\text{—Ph—}CO_3^\bullet]}{dt} = k_{11}[\mathrm{O_2}][m\text{—}CH_3\text{—Ph—}CO^\bullet] - (k_{12}[\mathrm{Co}^{2+}][\mathrm{H}^+] + k_{13}[\mathrm{Mn}^{2+}][\mathrm{H}^+] + k_{18}[\mathrm{Br}^\bullet])[m\text{—}CH_3\text{—Ph—}CO_3^\bullet] \tag{53}$$

From reactions (29), (30), and (33), the generating rate of $m\text{—HOOC—Ph—}RCH_2^\bullet$ radical may be determined as

$$\frac{d[m\text{—HOOC—Ph—}CH_2^\bullet]}{dt} = k_{19}[m\text{—TA}][\mathrm{Br}^\bullet] - (k_{20}[\mathrm{O_2}] + k_{23}[\mathrm{Br}^\bullet])[m\text{—HOOC—Ph—}CH_2^\bullet] \tag{54}$$

From reactions (30)–(32) and (34), the generating rate of $m\text{—}CH_3\text{—Ph—}RCH_2O_2^\bullet$ radical may be determined as

$$\frac{d[m\text{—HOOC—Ph—}CH_2O_2^\bullet]}{dt} = k_{20}[\mathrm{O_2}][m\text{—HOOC—Ph—}CH_2^\bullet] - (k_{21}[\mathrm{Co}^{2+}][\mathrm{H}^+] + k_{22}[\mathrm{Mn}^{2+}][\mathrm{H}^+] + k_{24}[\mathrm{Br}^\bullet])[m\text{—HOOC—Ph—}CH_2O_2^\bullet] \tag{55}$$

From reactions (35), (36), and (42), the generating rate of $m\text{—HOOC—Ph—}CO^\bullet$ radical may be determined as

$$\frac{d[m\text{—HOOC—Ph—}CO^\bullet]}{dt} = k_{25}[m\text{—CBA}][\mathrm{Br}^\bullet] - (k_{26}[\mathrm{O_2}] + k_{32}[\mathrm{Br}^\bullet])[m\text{—HOOC—Ph—}CO^\bullet] \tag{56}$$

From reactions (36)–(38) and (43), the generating rate of $m\text{—HOOC—Ph—}CO_3^\bullet$ radical may be determined as

$$\frac{d[m\text{—HOOC—Ph—}CO_3^\bullet]}{dt} = k_{26}[\mathrm{O_2}][m\text{—HOOC—Ph—}CO^\bullet] - (k_{27}[\mathrm{Co}^{2+}][\mathrm{H}^+] + k_{28}[\mathrm{Mn}^{2+}][\mathrm{H}^+] + k_{33}[\mathrm{Br}^\bullet])[m\text{—HOOC—Ph—}CO_3^\bullet] \tag{57}$$

From reactions (22)–(26), the generating rate of aromatic peroxyacid $m\text{—}CH_3\text{—Ph—COOOH}$ may be determined as

$$\frac{d[m\text{—}CH_3\text{—Ph—}CO_3\mathrm{H}]}{dt} = (k_{12}[\mathrm{Co}^{2+}][\mathrm{H}^+]) + k_{13}[\mathrm{Mn}^{2+}][\mathrm{H}^+])[m\text{—}CH_3\text{—Ph—}CO_3^\bullet] - (k_{14}[m\text{-TALD}] + k_{15}[\mathrm{Co}^{2+}]^2[\mathrm{H}^+]^2 + k_{16}[\mathrm{Mn}^{2+}]^2[\mathrm{H}^+]^2)[m\text{—}CH_3\text{—Ph—}CO_3\mathrm{H}] \tag{58}$$

From reactions (37)–(41), the generating rate of aromatic peroxyacid *m*—HOOC—Ph—COOOH may be determined as

$$\frac{d[m\text{—HOOC—Ph—CO}_3\text{H}]}{dt} = (k_{27}[\text{Co}^{2+}][\text{H}^+] + k_{28}[\text{Mn}^{2+}][\text{H}^+])[m\text{—HOOC—Ph—CO}_3^\bullet] - (k_{29}[m\text{-CBA}] + k_{30}[\text{Co}^{2+}]^2[\text{H}^+]^2 + k_{31}[\text{Mn}^{2+}]^2[\text{H}^+]^2)[m\text{—HOOC—Ph—CO}_3\text{H}] \quad (59)$$

Theoretically from Eqs. 48–59, the evolution relations of concentrations for radicals and peroxyacids coupled with time can be obtained. If substituting these relations into Eqs. 44–47, the detailed mechanistic kinetic models can be obtained. However, the models obtained in this manner are too complex and difficult to be used practically. Some simplifications are necessary and the following assumptions are made:

a. The quasi-steady-state approximation is used for these radicals and aromatic peracids. This means the differential items in the left side of Eqs. 48–59 can be assumed to be zero, and the total radical concentrations in Eq. 49 can be approximately a constant, i.e.

$$[\text{I}^\bullet] = \varepsilon \quad (60)$$

From Eqs. 48 and 60, by using the quasi-steady-state approximation, we can get

$$[\text{Br}^\bullet] = \frac{k_1[\text{Co}^{3+}] + k_3[\text{Mn}^{3+}]}{k_4[\text{MX}] + k_{10}[m\text{-TALD}] + k_{19}[m\text{-TA}] + k_{25}[m\text{-CBA}] + \varepsilon}[\text{Br}^-] \quad (61)$$

Inserting Eq. 61 into Eqs. 44 and 46, we can get the mechanism kinetic model for the oxidation of methyl to aldehyde group in the oxidation of MX to MPA as

$$r_1 = k_4[\text{MX}][\text{Br}^\bullet] = \frac{f_1(\text{T, Co, Mn, Br})[\text{MX}]}{k_4[\text{MX}] + k_{10}[m\text{-TALD}] + k_{19}[m\text{-TA}] + k_{25}[m\text{-CBA}] + \varepsilon} \quad (62)$$

$$r_3 = k_{19}[m\text{-TA}][\text{Br}^\bullet] = \frac{f_3(\text{T, Co, Mn, Br})[m\text{-TA}]}{k_4[\text{MX}] + k_{10}[m\text{-TALD}] + k_{19}[m\text{-TA}] + k_{25}[m\text{-CBA}] + \varepsilon}$$

b. Because oxidation operates at high oxygen pressure, the concentration of oxygen in liquid may be much higher than that for $\text{Br}^\bullet$ radical, i.e. $[\text{O}_2] >> [\text{Br}^\bullet]$;

c. The products of chain termination reactions (18)–(19), (27)–(28), (33)–(34), and (42)–(43) are side or by-products, which are in low concentrations compared with the main reaction products such as *m*-TALD or *m*-PT. The concentrations of these by-products are assumed negligible. By this assumption, the items represent termination reactions in Eqs. 48–59 can be neglected.

By using these three assumptions, the concentrations of peroxyacids produced in the oxidation process can be obtained from Eqs. 48–59, and the obtained expressions are shown in the following equation.

$$[m\text{—CH}_3\text{—Ph—CO}_3\text{H}] = \frac{k_{10}(m\text{-TALD}]}{k_{14}[m\text{-TALD}] + k_{15}[\text{Co}^{2+}]^2[\text{H}^+]^2 + k_{16}[\text{Mn}^{2+}]^2[\text{H}^+]^2}[\text{Br}^\bullet]$$
$$[m\text{—HOOC—Ph—CO}_3\text{H}] = \frac{k_{25}(4\text{-CBA}]}{k_{29}[m\text{-CBA}] + k_{30}[\text{Co}^{2+}]^2[\text{H}^+]^2 + k_{31}[\text{Mn}^{2+}]^2[\text{H}^+]^2}[\text{Br}^\bullet] \quad (63)$$

Inserting Eqs. 61 and 63 into Eqs. 45 and 47, we can get the mechanism kinetic model for the oxidation of aldehyde to carboxylic group in the oxidation of MX to MPA as

$$r_2 = \left(1 + \frac{k_{14}(m\text{-TALD}]}{k_{14}[m\text{-TALD}] + k_{15}[\text{Co}^{2+}]^2[\text{H}^+]^2 + k_{16}[\text{Mn}^{2+}]^2[\text{H}^+]^2}\right) \frac{f_2(\text{T, Co, Mn, Br})[m\text{-TALD}]}{k_4[\text{MX}] + k_{10}[m\text{-TALD}] + k_{19}[m\text{-TA}] + k_{25}[m\text{-CBA}] + \varepsilon}$$
$$r_4 = \left(1 + \frac{k_{29}(4\text{-CBA}]}{k_{29}[m\text{-CBA}] + k_{30}[\text{Co}^{2+}]^2[\text{H}^+]^2 + k_{31}[\text{Mn}^{2+}]^2[\text{H}^+]^2}\right) \frac{f_4(\text{T, Co, Mn, Br})[m\text{-CBA}]}{k_4[\text{MX}] + k_{10}[m\text{-TALD}] + k_{19}[m\text{-TA}] + k_{25}[m\text{-CBA}] + \varepsilon} \quad (64)$$

Equations 62 and 64 are the kinetic models for the reaction steps shown in Figure 1. Comparing Eq. 64 with Eq. 62, we can find the oxidation rate of aldehyde group is not only affected by the concentration of $\text{Br}^\bullet$ radical, but also affected by concentrations of peroxyacids. The oxidation aromatic aldehyde to aromatic acid has two sideways, one is the self-catalyzed Baeyer-Villiger reaction, [Reactions (24) and (39)], the other is the reduction of peroxyacid by Co(II) or Mn(II) [Reactions (25)–(26) and (40)–(41)]. In the recent works of Wang, the similar equation as Eq. 64 was also obtained for the oxidation of *para*-xylene to terephthalic acid. In that work, Eq. 64 was empirically expressed by the following equation[39,40]

$$r_2 = \frac{f_2(\text{T, Co, Mn, Br})[m\text{-TALD}]^\alpha}{k_4[\text{MX}] + k_{10}[m\text{-TALD}] + k_{19}[m\text{-TA}] + k_{25}[m\text{-CBA}] + \varepsilon}$$
$$r_4 = \frac{f_4(\text{T, Co, Mn, Br})[m\text{-CBA}]^\beta}{k_4[\text{MX}] + k_{10}[m\text{-TALD}] + k_{19}[m\text{-TA}] + k_{25}[m\text{-CBA}] + \varepsilon} \quad (65)$$

By combining the results from semi-continuous and batch experiments, the optimal α and β for the oxidation of *para*-xylene to terephthalic acid parameters are all approximately to be 1.[39,40] It indicated that although two oxidation sideways might occur to produce carboxylic acid in the oxidation of

aromatic hydrocarbon to aromatic acid, only one sideway reaction might be dominated in specific operation conditions. The oxidations of MX to MPA and the oxidation of *para*-xylene to terephthalic acid both belongs to the aromatic hydrocarbon oxidation to aromatic acid, and for the generating of carboxylic group from aldehyde group in the oxidation of MX to MPA, we could also expect that only one sideway reaction might be dominated in specific operation oxidation conditions. That is to say, we can expect the following kinetic model for the oxidation of aldehyde group to carboxylic group

$$r_2 = \frac{f_2(\mathrm{T},\mathrm{Co},\mathrm{Mn},\mathrm{Br})[m\text{-TALD}]}{k_4[\mathrm{MX}] + k_{10}[m\text{-TALD}] + k_{19}[m\text{-TA}] + k_{25}[m\text{-CBA}] + \varepsilon}$$

$$r_4 = \frac{f_4(\mathrm{T},\mathrm{Co},\mathrm{Mn},\mathrm{Br})[m\text{-CBA}]}{k_4[\mathrm{MX}] + k_{10}[m\text{-TALD}] + k_{19}[m\text{-TA}] + k_{25}[m\text{-CBA}] + \varepsilon} \tag{66}$$

From Eqs. 62 and 66, the kinetic model for reactions in the MX liquid-phase catalytic oxidation to MPA can be obtained in the following general expression

$$r_i = k_i c_i[\mathrm{Br}^\bullet] = \frac{k_i c_i}{\lambda_1 c_1 + \lambda_2 c_2 + \lambda_3 c_3 + \lambda_4 c_4 + \varepsilon} \quad i = 1-4 \tag{67}$$

where ε and λ_i are model parameters, and are independent of catalyst concentrations. k_i is the reaction rate constant, and factors affecting k_i are temperature, solvent composition, catalyst concentration, and catalyst ratios Co/Mn and Br/(Co+Mn). Comparing model Eq. 67 with the empirical model Eq. 1, we find the number of model parameters needed to be regressed are greatly decreased from 28 to 9 at a certain operation condition, and the nine model parameters can easily be uniquely determined by data fitting.

Mechanistic model Eq. 67 is a radical competition model and reveals the following the special competition mechanism. Radical $Br^\bullet$ is a key factor to initiate the oxidation process, and its concentration determines the reaction rate directly. When the concentration of reactants increases, from Eq. 61 we can see that the concentration of radical $Br^\bullet$ decreases, which restricts the acceleration of the reaction rate. When the concentration of reactants decreases, from Eq. 61 we can see that the concentration of radical $Br^\bullet$ increases, which restricts the deceleration of the reaction rate. Because of the restriction effect of radical $Br^\bullet$, the change of apparent reaction rate is not sensitive with the change of reactants concentration. This unique characteristic is consistent with the large quantity of experimental data in our group for aromatic hydrocarbon oxidation to aromatic acid.[25,26,29,30,39,40]

Reactor Models

By taking into account only the formation of the molecular species that represented the most important intermediate and final product, the lumped kinetic scheme as shown in Figure 1 and the kinetic model of Eq. 67 was used. The description of the diffusion and reaction processes at the gas–liquid interface was neglected because of the elimination of mass transfer influence, which will be further proved in the following section. Because all experiments were performed under the kinetic regime, the following mass balances were used:

$$\frac{dc_j}{dt} = \sum_{i=1}^{4} v_{i,j} r_j \quad j = 1-4 \tag{68}$$

along with the initial conditions

$$c_j = c_{j,0} \quad j = 1-4 \tag{69}$$

The energy balance was not considered here, because the reactor had been operated under isothermal conditions. The kinetic parameters were determined in a nonlinear optimization, minimizing the difference between the simulated and the experimental time evolution of the product composition of experimental runs 1–6. The fourth-order Runge-Kutta method was used to discrete Eq. 68, and the simplex method was used in the nonlinear optimizations. The method is implemented in the Matlab Optimization Toolbox (The Mathworks). The simulation was written in Matlab to use their optimization routine.

Results and Discussion

Confirmation of the reaction scheme

First, experimental run 2 is carried out to confirm the reaction scheme. The experimental results are plotted in Figure 4. It shows that the concentration of each intermediate first increases to a maximum value and then decreases. The concentration of reactant MX decreases monotonically, and the total concentration of product MPA increases monotonically. These are all the typical characteristic of consecutive reactions. From the sequence each reactants increase and decrease, we can conclude that the first methyl group of MX is first oxidized to aldehyde (*m*-TALD) and acid (*m*-TA). At the three-seventh time of the total batch reaction time, the

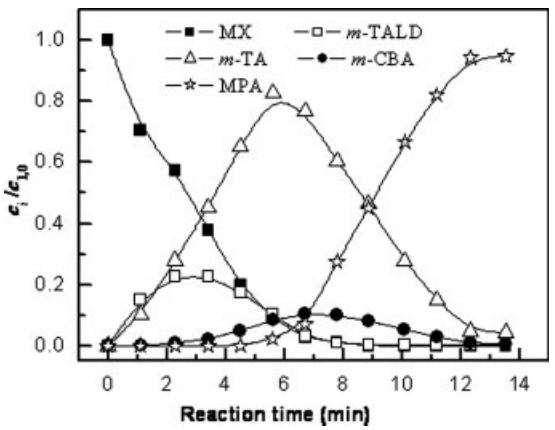

Figure 4. The time evolution of liquid reactant and intermediates concentrations at initial MX/HAc(mass ratio) = 0.10 and stirring rate 900 rpm and temperature 463.2 K (Run 2).

Symbols are for experimental results, and line is for model-fitted results.

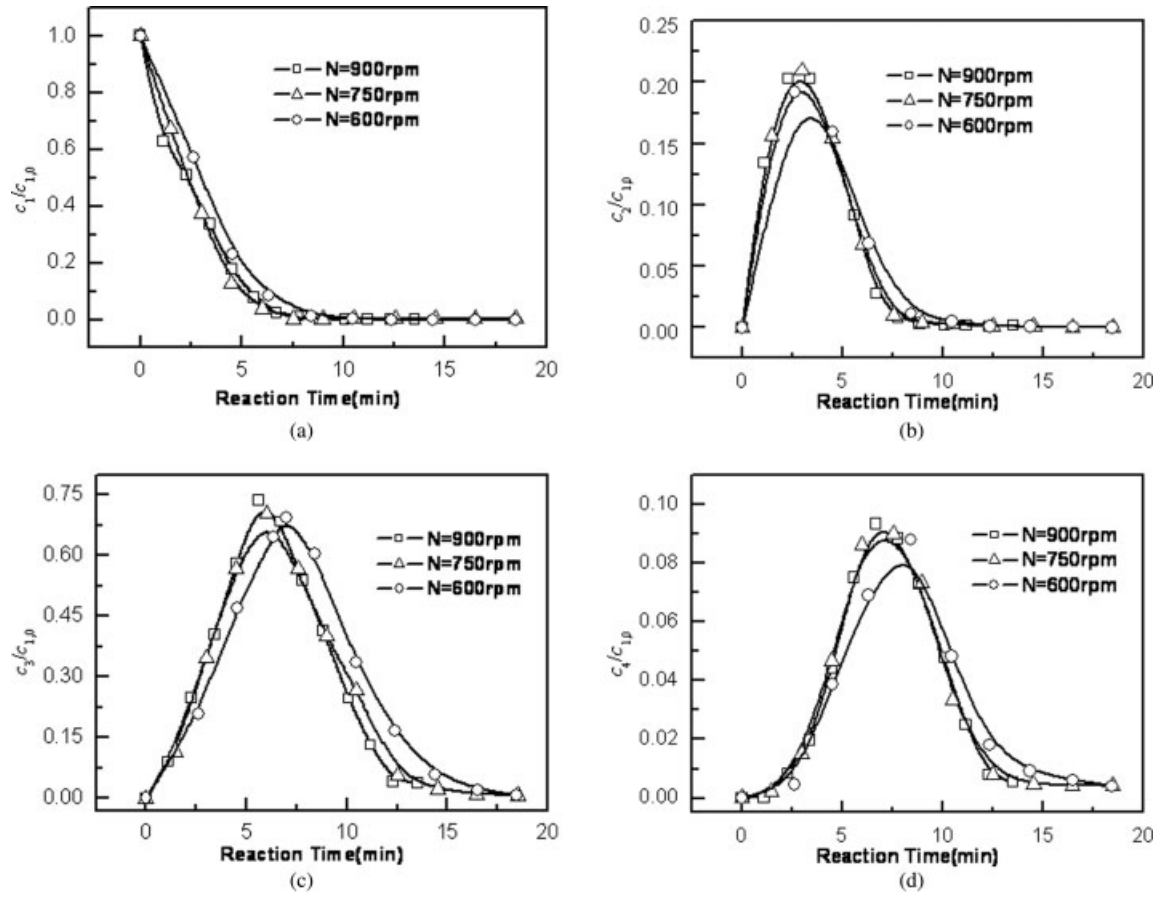

Figure 5. The time evolution of liquid reactant and intermediates concentrations with variation of stirring rate 600, 750, and 900 rpm at 463.2 K and initial MX/HAc(mass ratio) = 0.10 (Runs 2, 7, 8).

a is for MX, b is for *m*-TALD, c is for *m*-PT, and d is for *m*-CBA.

first methyl is almost completely oxidized. The concentration of *m*-TA reaches a maximum value, and the second methyl group is followed to be oxidized, which is a relatively slower process. During this course, the second methyl group is oxidized to aldehyde (*m*-CBA) and then *m*-CBA to acid (MPA). The experimental results shown in Figure 4 confirm that the reaction scheme of MX liquid-phase catalytic oxidation to MPA can be determined as that shown in Figure 1.

Effect of stirring rate

To obtain the intrinsic reaction kinetics, the elimination of gas–liquid mass transfer on the oxidation process is necessary. In this work, we intensified the gas–liquid mass transfer by increasing the stirring rate. Experimental runs 2 and 7–8 were carried out to determine the effect of stirring rate on the oxidation process. The experimentally determined evolutions of MX, *m*-TALD, *m*-PT, and *m*-CBA concentrations in solution with time are plotted in Figure 5.The experimentally determined concentration evolution curve for any of the reactant and intermediates is almost overlapped at 750 rpm and 900 rpm, which clearly shows that the effect of stirring rate on the component concentrations in solution is insignificant when the stirring rate is higher than 750 ppm, and the MX oxidation process is controlled by chemical reactions. The influences of mass transfer and gas–liquid mixing on the oxidation process are negligible under the studied experimental conditions. In the section "Reactor Model", the assumption that the description of the diffusion and reaction processes at the gas–liquid interface is negligible because of the elimination of mass transfer influence is reasonable. To ensure the effect of gas–liquid mass transfer on the reaction process can be neglected, the experimental runs to study the kinetics of MX oxidation to MPA are chosen to be carried out at 900 rpm.

Kinetics parameters evaluation

The time evolution of experimentally determined concentration for major reactants and intermediates MX, *m*-TALD, *m*-TA, and *m*-CBA with variation of initial MX/HAc(mass ratio) = 0.20, 0.10, and 0.05 at 463.2 K and stirring rate 900 rpm (Runs 1, 2, 3) were plotted in Figure 6.

The time evolution of liquid reactant and intermediates concentrations with variation of reaction temperature 453.2, 458.2, 463.2, and 468.2 K at initial MX/HAc(mass ratio) = 0.10 and stirring rate 900 rpm (Runs 4, 2, 5, 6) were plotted in Figure 7.

When kinetic model Eq. 67 and reactor model Eqs. 68 and 69, accompanied with the experimental data shown in Figures 6 and 7, are used to determine the model parameters,

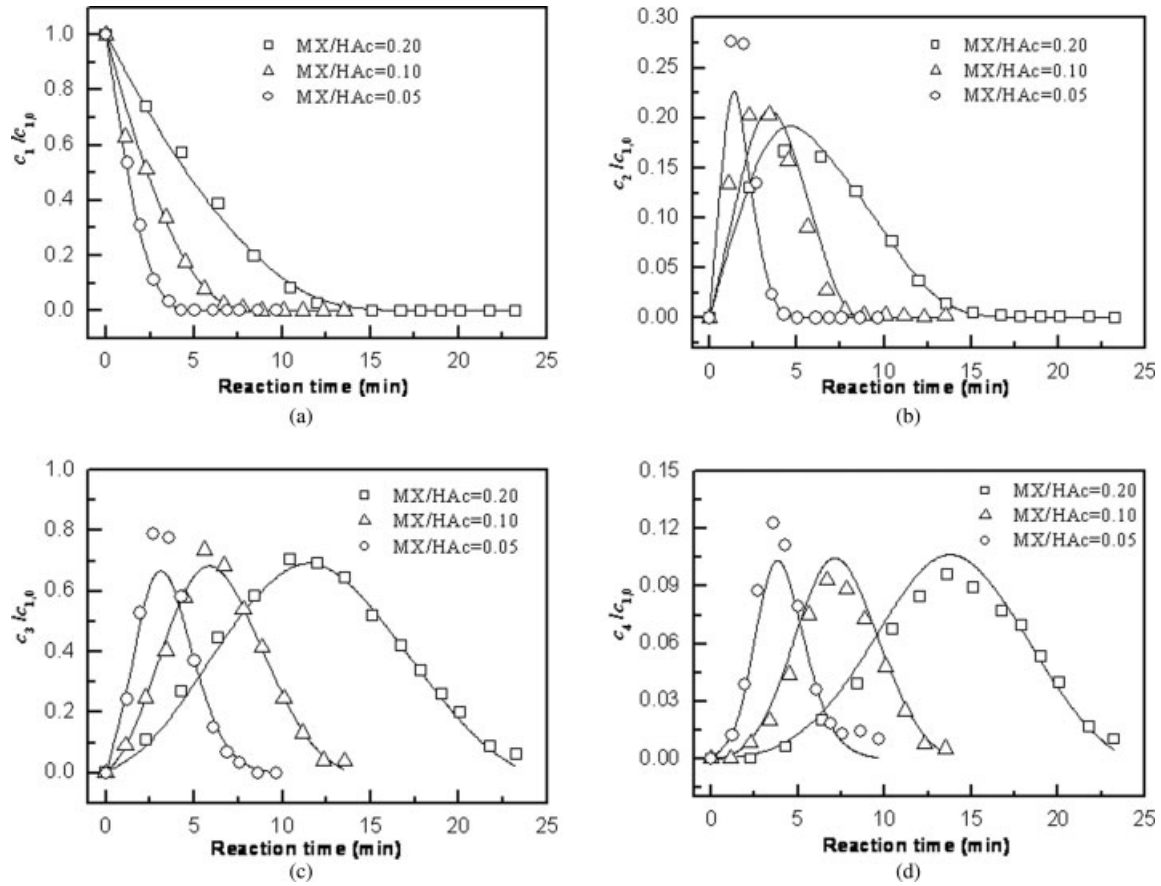

Figure 6. The time evolution of liquid reactant and intermediates concentrations with variation of initial MX/HAc (mass ratio) = 0.20, 0.10, and 0.05 at 463.2 K and stirring rate 900 rpm (Runs 1, 2, 3).

a is for MX, b is for *m*-TALD, c is for *m*-PT, and d is for *m*-CBA. Symbols are for experimental results, and line is for model fitted results.

we find that the activation energy for different reaction step is almost the same. Considering this, we assumed the following Arrhenius equation to represent the effect of temperature on the reaction

$$k_i = k_{i0} \exp(-E_a/RT) \tag{70}$$

We noticed that in the oxidation of *para*-xylene to terephthalic acid, Eq. 70 was also used to correlate the effect of temperature on the reaction rate constant.[29,39,40] The experimental results shown in Figures 6 and 7 are put together to simultaneously determine the reaction model parameters by minimizing the difference between the calculated reactants concentrations and the experimentally determined reactants concentrations. The model parameters for MX oxidation to MPA are determined and given in Table 2.

A comparison between the simulated results and the experimental data is also plotted in Figure 6 and 7, where it can be seen that the obtained agreement is in general satisfactory. The average relative deviation of the simulated value and the experimental data for most of the experimental points is $<5\%$. This model is able to predict the reactor behavior as functions of the temperature and the concentration of the liquid reactants.

Discussion

After smoothing the experimentally determined MX concentration curve for experimental run 1–3, we obtained the oxidation rate $r_1 = dc_1/dt$ for MX oxidation to *m*-TALD by numerical difference. The experimentally determined r_1 at different initial MX concentration (Runs 1, 2, 3) are plotted in Figure 8. The calculated results using the kinetic model Eq. 67 and the model parameters given in Table 2 are also given in Figure 8 using line. According to the empirical *n*-th order kinetics, the reaction rate is one-to-one corresponded with the reactant concentration. However, the results illustrated in Figure 8 show that one reactant concentration might be corresponded with different reaction rate at different experimental run. The phenomenon is obviously contradictory to the experimental resulted predicted by empirical *n*-th order kinetics, which means the empirical *n*-th order kinetics does not reveal the reaction mechanism sufficiently. However, the experimentally determined and model calculated evolution of oxidation rate for MX to *m*-TALD with the concentration of MX for experimental run 1–3 are in good agreement, which means the kinetic model Eq. 67 reveals the reaction mechanism sufficiently.

Taking $c_1 = 0.15$ mol/kg$_{HAc}$ (Point A) as example, the reaction rate r_1 is 0.125 (Point B) for experimental run 3,

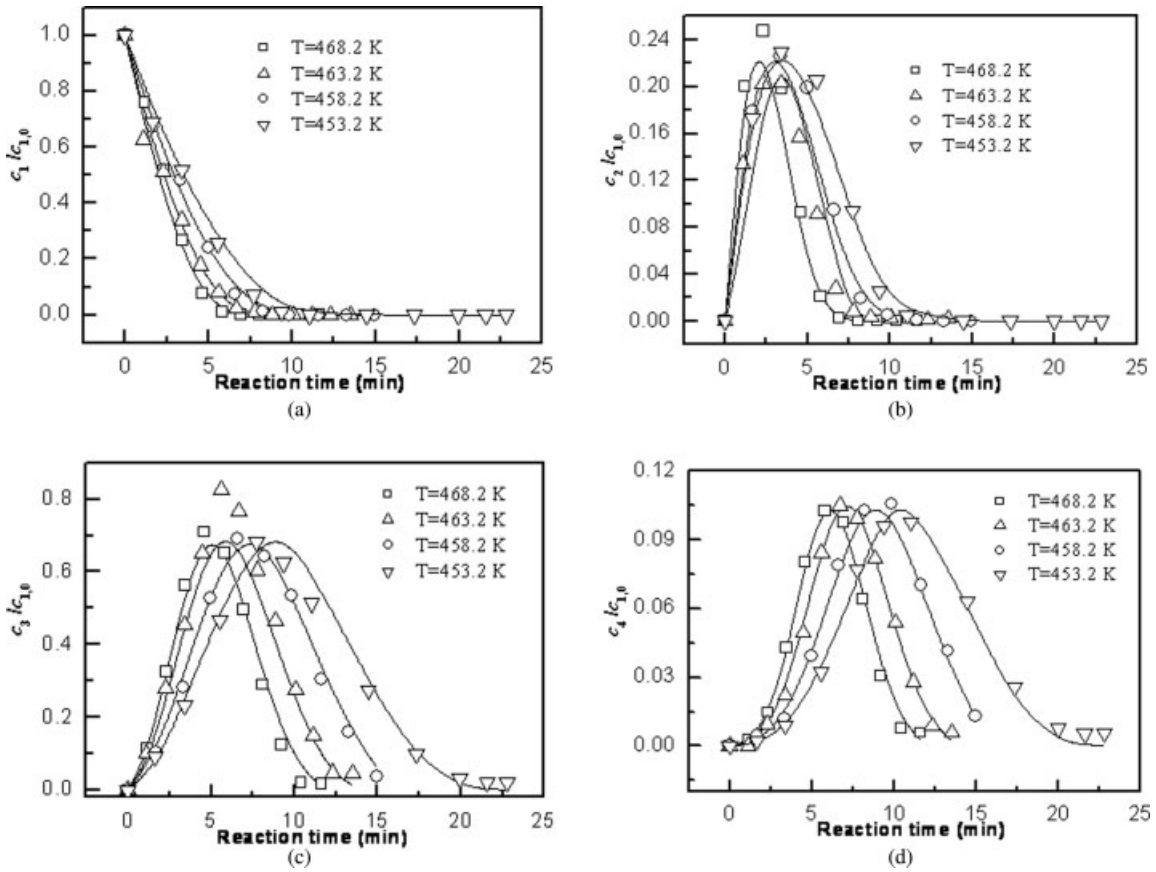

Figure 7. The time evolution of liquid reactant and intermediates concentrations with variation of reaction temperature 453.2, 458.2, 463.2, and 468.2 K at initial MX/HAc(mass ratio) = 0.10 and stirring rate 900rpm (Runs 4, 2, 5, 6).

a is for MX, b is for *m*-TALD, c is for *m*-PT and d is for *m*-CBA. Symbols are for experimental results, and line is for model fitted results.

0.095 (Point C) for experimental run 2, and 0.070 (Point D) for experimental run 1. The difference of r_1 at the same concentration of MX for different experimental run can be interpreted by the model Eq. 67. Kinetic model Eq. 67 shows that r_1 is affected not only by the concentration of MX, but also by the concentrations of other intermediates produced during the oxidation process. From Figure 6, we can see that the denominator in Eq. 67, representing a linear summation of concentrations for MX, *m*-TALD, *m*-TA, and *m*-CBA, is the biggest for experimental run 1, and smallest for experimental run 3. It means that although the numerator (the concentration of MX) is the same, the reaction rate is the smallest for experimental run 1, and biggest for experimental run 3. The same experimental phenomenon was also found in the oxidation of *para*-xylene to terephthalic acid.[25,26,29,30,39,40]

Table 2. Model Parameters in Eqs. 67 and 70

	$i = 1$	$i = 2$	$i = 3$	$i = 4$
$10^{-7}\ k_{i0}$	4.281	9.133	0.629	3.668
λ_i	12.25	7.05	2.53	0.0788
ε		0.30		
E_a		63.6		

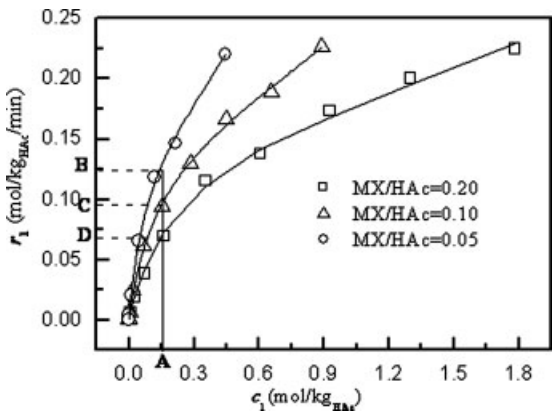

Figure 8. The oxidation rate for *meta*-xylene with the concentration variation of *meta*-xylene at initial MX/HAc(mass ratio)=0.20, 0.10, 0.05 and stirring rate 900rpm and temperature 463.2K (Runs 1,2,3).

Symbols are for experimental results, and line is for model-fitted results.

From Figure 8, we can get the initial reaction rate r_1 at different initial MX concentration and it is shown in Table 3. Another interesting experimental phenomenon was found. At $t = 0$, the concentrations of intermediates were zero, and the only reactant was MX. From Table 3, we can see that from experimental run 3 to 1, the concentration of MX (c_1) increased 300%, while the oxidation rate of MX (r_1) increased less than 5%. The reaction rate is not sensitive with the concentration of reactant. The interesting phenomenon also cannot be interpreted by the empirical *n*-th order kinetics, but can be well interpreted by the kinetic model Eq. 67.

The chemical reason for the unusual concentration dependence illustrated in Figure 8 and Table 3 might because of changes in the concentration of benzylic bromides that form. The benzylic bromides are an inactive form of bromide, i.e. it is not a catalyst. When they form they change the Br/(Co + Mn) ratio, which changes the rate of reaction. This has been experimentally demonstrated in detail in Ref. 18. In this work, we have explicitly included the formation of benzylic bromides in reactions (18) and (33). Hence it would be reasonable that the kinetic model Eq. 67 derived from the free-radical chain reaction mechanism can account for the unusual rate dependence on the concentration of MX, and the other empirical *n*-th kinetic models might be failed.

Mechanistic model Eq. 67 is a radical competition model and reveals that radical $Br^{\bullet}$ is a key factor to initiate the oxidation process, and its concentration determines the reaction rate directly. When the concentration of reactants increases, from Eq. 67 we can see the concentration of radical $Br^{\bullet}$ decreases, which restricted the acceleration of reaction rate. When the concentration of reactants decreases, from Eq. 67 we can see the concentration of radical $Br^{\bullet}$ increases, which restricted the deceleration of reaction rate. Because of the restriction effect of radical $Br^{\bullet}$, the change of apparent reaction rate is not sensitive with the change of reactants concentration. This unique character is consistent with the large quantity of experimental data in our group,[3] and also has been found in the oxidation of *para*-xylene to terephthalic acid.[25,26,29,30,39,40] Furthermore, based on model Eq. 67 and the determined model parameters, the simulation results for industrial oxidation reactor agree well with the plant field data.[3]

The reaction rate constants for the reaction steps in Figure 1 for experimental run 2 are shown in Table 4. From Table 4, three interesting results can be obtained. (1) The reaction of *m*-TA to *m*-CBA is the slowest step and the rate controlling step of the process. This result is valuable for the reaction intensification, and it directed out that the intensification of *m*-TA oxidation to *m*-CBA is most important for the oxidation process intensification. Similar result has also been obtained in the oxidation of *para*-xylene to terephthalic acid.[14–18,25,26,29,30] (2) The reactivity of MX/*m*-PT is about 7, and the reactivity of *m*-TALD/*m*-CBA is about 2.5, which are all consistent with the predicted rate ratio by the Hammett function proposed by Partenheimer. Here, we must emphasis that the rate information from the Hammett equation is based on experimental data[14] (3) The oxidation of second methyl or aldehyde group is more difficult than the first methyl or aldehyde group. It might be due to the electrophilic effect resulted by the *meta*-carboxylic group, which resulted that the second methyl or aldehyde group is more difficult to be oxidized. In the oxidation of *para*-xylene to terephthalic acid,[25,26,29,30,39,40] we also found the three interesting results.

Table 3. The Initial Oxidation Rate of *meta*-Xylene at Different Initial *meta*-Xylene Concentration

Experimental run	3	2	1
c_1	0.445	0.890	1.78
r_1	0.220	0.226	0.229

Table 4. The Reaction Rate Constants for the Reactions of MX to *m*-TALD (k_1), *m*-TALD to *m*-PT (k_2), *m*-PT to *m*-CBA (k_3), and *m*-CBA to MPA (k_4) at the Stirring Rate 900 rpm and Reaction Temperature 463.2 K (Run 2)

I	1	2	3	4
k_i	2.849	6.079	0.419	2.442

Conclusions

Some kinetic aspects of the air oxidation of *meta*-xylene to *meta*-phthalic acid in acetic acid in the temperature range from 453.2 to 468.2 K, catalyzed by cobalt acetate and manganese acetate and promoted by hydrogen bromide (HBr), are examined. This work consists of two parts. In the first part, a detailed radical chain elementary reaction mechanism for the liquid-phase catalytic oxidation of *meta*-xylene to *meta*-phthalic acid is proposed. Using several assumptions a simple fractional-like kinetic model is derived from the assumed reaction mechanism. In the second part, several batch oxidation experiments are carried out to study the oxidation kinetics. The experiments included three values of the initial *meta*-xylene concentrations and four values of reaction temperature. The developed model parameters were determined in a nonlinear optimization, minimizing the difference between the simulated and experimental time evolutions of the product compositions experimentally obtained in a batch oxidation reactor, where the gas and liquid phases were well mixed. A comparison between the simulated results and the experimental data showed the obtained agreement is in general satisfactory. This model is able to predict the reactor behavior as functions of the temperature and the concentration of the liquid reactants.

The experimental results cannot be interpreted by the empirical *n*-th order kinetics, but can be interpreted by the kinetic model proposed in this work. It means the kinetic model proposed in this work reveals the reaction mechanism.

Acknowledgments

Some of the experimental data are cited from the published work in literature 2 and 3. The authors thank Zhang, Y. Z., Ding, G. H., and Luo, X. F. for their fine and hard experiment work. They also thank Dr. Partenheimer, W. for his valuable comments on the reaction mechanism.

Notation

c_i = concentration of *i*th component, mol/kg_{HAc}
$c_{i,0}$ = initial concentration of *i*th component, mol/kg_{HAc}
d_{ij} = model parameters in Eq. 1
E_a = the activation energy defined by Eq. 70, kJ/ mol

k_i = the rate constants, min^{-1}
$k_{i,0}$ = the rate constants defined by Eq. 70, min^{-1}
r_i = rate of the ith step reaction, mol/(kg_{HAc} · min)

Greek letters

β = model parameters in Eq. 1
ε = model parameters in Eqs. 1 and 67
v_{ij} = stoichiometric coefficient of the jth component in the ith reaction
λ = model parameters in Eq. 67

Abbreviations

m-CBA = *meta*-carboxybenezaldehyde
m-TA = *meta*-toluic acid
MX = *meta*-xylene
MPA = *meta*-phthalic acid
m-TALD = *meta*-tolualdehyde
DMSO = dimethyl sulfoxide
IPB = isopropyl benzene
HPLC = high-performance liquid chromatograph
GC = gas chromatograph
HAc = acetic acid

Literature Cited

1. Zhang Z. *Study on the Kinetics of Catalytic Liquid-Phase Oxidation of m-Xylene*, M.S. Thesis, East China University of Science and Technology, Shanghai, P.R. China, 2003.
2. Zhang YZ, Li X, Ding GH, Cheng YW. Kinetics of liquid phase catalytic oxidation of *m*-xylene to isophthalic acid. *Chem React Eng Technol*. 2006;22:97–102.
3. Zhang YZ. *Kinetics of Liquid Phase Catalytic Oxidation of m-Xylene and Co-Oxidation of C8 Aromatic Hydrocarbons*. M.S. Thesis, Zhejiang University, Hangzhou, P.R. China, 2006.
4. Wan J. *Study on Liquid-Phase Catalytic Oxidation of m-Xylene to Isophthalic Acid*, M.S. Thesis, East China University of Science and Technology, Shanghai, P.R. China, 2004.
5. Kamiya Y. Catalysis by cobalt and bromide ions in the autoxidation of alkyl benzenes in acetic acid. *J Catal*. 1974;33:480–485.
6. Hendriks C, Beek H, Heertjes P. Reactions of some peracids and hydroperoxides with cobalt(II) and cobalt(III) acetate in acetic acid solution. *Ind Eng Chem Prod Res Dev*. 1979;18:38–43.
7. Jones GH. *p*-Xylene autoxidation studies: oxidation of cobalt(II) and manganese(II) acetates by peracids. *J Chem Soc Chem Commun*. 1979;12:536–537.
8. Jones GH. A Kinetic and mechanistic study of the redox chemistry of cobalt acetate in aqueous acetic acid. *J Chem Res*. 1981;7:2801–2868.
9. Jones GH. A mechanistic study of the origin of synergy and antagonism in the Co(OAc)Br-catalyzed autoxidation of *p*-xylene. *J Chem Res*. 1981;8:2137–2163.
10. Hronec M, Cvengrosova Z, Ilsvsky J. Kinetic and mechanistic of cobalt-catalyzed oxidation of *p*-xylene in the presence of water. *Ind Eng Chem Prod Res Dev*. 1985;24:787–794.
11. Hronec M, Hrabe Z. Liquid-phase oxidation of *p*-xylene catalyzed by metal oxides. *Ind Eng Chem Prod Res Dev*. 1986;25:257–261.
12. Partenheimer W. Characterization of the reaction of cobalt(II) acetate, dioxygen and acetic acid, and its significance in autoxidation reactions. *J Mol Catal*. 1991;67:35–46.
13. Partenheimer W, Gipe RK. Kinetics and thermodynamics of the reactions of Co(OAC)2, Mn(OAC)2 and bromide salts with *m*-chloroperbenzoic acid (MCPBA) in acetic acid. *Div Petrol Chem Am Chem Soc*. 1992;37:1098–1104.
14. Partenheimer W. Methodology and scope of metal/bromide autoxidation of hydrocarbons. *Catal Today*. 1995;23:69–158.
15. Partenheimer W. The structure of metal/bromide catalysts in acetic acid/water mixtures and its significance in autoxidation. *J Mol Catal A: Chem*. 2001;174:29–33.
16. Partenheimer W. A Chemical Model for the Amoco 'MC' Oxygenation Process to Produce Terephthalic Acid. In: Blackburn DW, editor. *Catalysis of Organic Reactions*, Chapter 20. New York: Marcel Dekker, 1990.
17. Partenheimer W. The effect of zirconium in metal/bromide catalysts on the autoxidation of *p*-xylene. I. Activation and changes in benzaldehyde intermediate formation, *J Mol Catal*. 2003;206:105–119.
18. Partenheimer W. The complex synergy of water in the metal/bromide autoxidation of hydrocarbons caused by benzylic bromide formation. *Adv Synth Catal*. 2004;346:297–306.
19. Suresh AK, Sharma MM, Sridhar T. Engineering aspects of industrial liquid-phase air oxidation of hydrocarbons. *Ind Eng Chem Res*. 2000;39:3958–3997.
20. Suresh AK, Sridhar T, Potter OE. Catalyzed oxidation of cyclohexane in the liquid phase. *AIChE J*. 1990;36:137.
21. Harustiak M, Hronec M, Ilsvsky J. Kinetics and mechanism of cobalt bromide catalyzed oxidation of *p*-xylene in the presence of phase transfer catalysts. *J Mol Catal*. 1989;53:209–217.
22. Harustiak M, Hronec M, Ilsvsky J. Kinetics and mechanism of phase-transfer catalyzed oxidation of *p*-xylene by molecular oxygen. *J Mol Catal*. 1988;48:335–342.
23. George WP, Steven DI. *Homogeneous Catalysis: The Applications and Chemistry of Catalysis by Soluble Transition Metal Complexes*, 2nd ed. Wiley: New York, 1992.
24. Sheldon AR, Kochi JK. *Metal-Catalyzed Oxidations of Organic Compounds: Mechanistic Principles and Synthetic Methodology Including Biochemical Processes*. New York: Academic Press, 1981.
25. Wang LJ. *Kinetics and Reactor Modeling for the Oxidation of p-Xylene to Terephthalic Acid*. M.S. Thesis, Zhejiang Univeristy, Hangzhou, China, 2001.
26. Wang LJ, Li X, Xie G, Cheng YW, Sima J. Studies on the kinetics of the *p*-xylene liquid phase catalytic oxidation (I): mechanism and kinetic model. *J Chem Ind Eng*. 2003;54:946–952.
27. Emanuel NM, Gal D. *Modelling of Oxidation Processes*. Budapest, Hungary: Akademiai Kiado, 1986.
28. Marta F, Boga E, Matic M. Interpretation of limiting rate and of induction period in oxidation of benzaldehyde catalyzed by cobaltous acetate. *Discuss Faraday Soc*. 1986;46:173.
29. Wang QB, Cheng YW, Wang LJ, Xu HB, Li X. Semi-continuous studies on the reaction mechanism and kinetic for the liquid-phase oxidation of *p*-xylene to terephthalic acid. *Ind Eng Chem Res*. 2007;46:8980–8992.
30. Cheng YW. *Studies on MC Process of Hydrocarbon Liquid Phase Catalytic Oxidation*. Ph.D. Dissertation, Zhejiang Univeristy, Hangzhou, China, 2004.
31. Raghavendrachar P, Ramachadran S. Liquid-phase catalytic oxidation of *p*-xylene. *Ind Eng Chem Res*. 1992;31:453–462.
32. Cao G, Massimo P, Massimo M. A lumped kinetic model for liquid-phase catalytic oxidation of *p*-xylene to terephthalic acid. *Chem Eng Sci*. 1994;49:5775–5783.
33. Cao G, Alberto S, Massimo P. Kinetics of *p*-xylene liquid-phase catalytic oxidation. *AIChE J*. 1994;40:1156–1166.
34. Cincotti A, Orru R, Bori A, Cao G. Effect of catalyst concentration and simulation of precipitation processes on liquid-phase catalytic oxidation of *p*-xylene to terephthalic acid. *Chem Eng Sci*. 1997;52:4205–4213.
35. Cincotti A, Orru R, Cao G. Kinetics and related engineering aspect of catalytic oxidation of *p*-xylene to terephthalic acid. *Catal Today*. 1999;52:331–347.
36. Holliday RL, Jong BWM, Kolis JW. Organic synthesis in subcritical water: oxidation of alkylaromatics. *J Supercrit Fluids*, 1998;12:1255.
37. Cheng YW, Zhang L, Xie G, Li X. Experimental technology of *p*-xylene liquid-phase catalytic oxidation. *Chem React Eng Technol*. 2003;19:182–187.
38. Partenheimer W. The complex synergy of water in metal/bromide autoxidations. II. Effect of water and catalyst on the aerobic oxidation of benzaldehydes and the effect of water on the elementary pathways. *Adv Synth Catal*. 2005;347:580–590.
39. Wang QB. *Reactive Crystallization in the Oxidation of p-Xylene*. Ph.D. Dissertation, Zhejiang University, Hangzhou, China, 2006.
40. Wang QB. *Reactive Crystallization in the High-Temperature Oxidation of p-Xylene to Terephthalic Acid*. Post-doctor Research Report, Zhejiang Univeristy, Hangzhou, China, 2008.

Manuscript received Oct. 27, 2007, and revision received Apr. 29, 2008.